

# Leading Order Analysis of Neutrino Induced Dimuon Events in the CHORUS Experiment

The CHORUS Collaboration

A. Kayis-Topaksu, G. Önengüt

Çukurova University, Adana, Turkey

R. van Dantzig, M. de Jong, R.G.C. Oldeman<sup>1</sup>

NIKHEF, Amsterdam, The Netherlands

M. Güler, S. Kama, U. Köse, M. Serin-Zeyrek, P. Tolun

METU, Ankara, Turkey

M.G. Catanesi, M.T. Muciaccia

Università di Bari and INFN, Bari, Italy

A. Bülte, K. Winter

Humboldt Universität, Berlin, Germany<sup>2</sup>

B. Van de Vyver<sup>3,4</sup>, P. Vilain<sup>5</sup>, G. Wilquet<sup>5</sup>

Inter-University Institute for High Energies (ULB-VUB) Brussels,  
Belgium

B. Saitta

Università di Cagliari and INFN, Cagliari, Italy

E. Di Capua

Università di Ferrara and INFN, Ferrara, Italy

S. Ogawa, H. Shibuya

Toho University, Funabashi, Japan

I.R. Hristova<sup>6</sup>, T. Kawamura, D. Kolev<sup>7</sup>, M. Litmaath, H. Meinhard,  
J. Panman, A. Rozanov<sup>8</sup>, R. Tsenov<sup>7</sup>, J.W.E. Uiterwijk, P. Zucchelli<sup>3,9</sup>

**CERN, Geneva, Switzerland**

J. Goldberg

**Technion, Haifa, Israel**

M. Chikawa

**Kinki University, Higashiosaka, Japan**

J.S. Song, C.S. Yoon

**Gyeongsang National University, Jinju, Korea**

K. Kodama, N. Ushida

**Aichi University of Education, Kariya, Japan**

S. Aoki, T. Hara

**Kobe University, Kobe, Japan**

T. Delbar, D. Favart, G. Grégoire, S. Kalinin, I. Makhlioueva

**Université Catholique de Louvain, Louvain-la-Neuve, Belgium**

A. Artamonov, P. Gorbunov, V. Khovansky, V. Shamanov, I. Tsukerman

**Institute for Theoretical and Experimental Physics, Moscow, Russian  
Federation**

N. Bruski, D. Frekers, D. Rondeshagen, T. Wolff

**Westfälische Wilhelms-Universität, Münster, Germany<sup>2</sup>**

K. Hoshino, J. Kawada, M. Komatsu, M. Miyanishi, M. Nakamura,  
T. Nakano, K. Narita, K. Niu, K. Niwa, N. Nonaka, O. Sato, T. Toshito

**Nagoya University, Nagoya, Japan**

S. Buontempo, A.G. Cocco, N. D'Ambrosio, G. De Lellis, G. De Rosa,  
F. Di Capua, G. Fiorillo, A. Marotta, M. Messina, P. Migliozi,  
R. Santorelli, L. Scotto Lavina, P. Strolin, V. Tioukov

Università Federico II and INFN, Naples, Italy

T. Okusawa

Osaka City University, Osaka, Japan

U. Dore, P.F. Loverre, L. Ludovici, G. Rosa, R. Santacesaria,  
A. Satta, F.R. Spada

Università La Sapienza and INFN, Rome, Italy

E. Barbuto, C. Bozza, G. Grella, G. Romano, C. Sirignano,  
S. Sorrentino

Università di Salerno and INFN, Salerno, Italy

Y. Sato, I. Tezuka

Utsunomiya University, Utsunomiya, Japan

---

<sup>1</sup> Now at University of Cagliari, Cagliari, Italy.

<sup>2</sup> Supported by the German Bundesministerium für Bildung und Forschung under contract numbers 05 6BU11P and 05 7MS12P.

<sup>3</sup> Now at SpinX Technologies, Geneva, Switzerland.

<sup>4</sup> Fonds voor Wetenschappelijk Onderzoek, Belgium.

<sup>5</sup> Fonds National de la Recherche Scientifique, Belgium.

<sup>6</sup> Now at DESY, Hamburg.

<sup>7</sup> On leave of absence and at St. Kliment Ohridski University of Sofia, Bulgaria.

<sup>8</sup> Now at CPPM CNRS-IN2P3, Marseille, France.

<sup>9</sup> On leave of absence from INFN, Ferrara, Italy.

---

## Abstract

We present a leading order QCD analysis of a sample of neutrino induced charged-current events with two muons in the final state originating in the lead-scintillating fibre calorimeter of the CHORUS detector. The results are based on a sample of 8910 neutrino and 430 antineutrino induced opposite-sign dimuon events collected during the exposure of the detector to the CERN Wide Band Neutrino Beam between 1995 and 1998. The analysis yields a value of the charm quark mass of  $m_c = (1.26 \pm 0.16 \pm 0.09) \text{ GeV}/c^2$  and a value of the ratio of the strange to non-strange sea in the nucleon of  $\kappa = 0.33 \pm 0.05 \pm 0.05$ , improving the results obtained in similar analyses by previous experiments.

*Key words:* Charm production, neutrino, dimuon

---

## Introduction

In neutrino-nucleon deep-inelastic scattering, events that present two muons in the final state are mainly due to the muonic decay of a charmed hadron produced in a neutrino charged-current interaction. The charm quark can be produced both through  $d \rightarrow c$  and  $s \rightarrow c$  weak currents. The  $\bar{s} \rightarrow \bar{c}$  transition dominates in the antineutrino induced dimuon events, whilst in neutrino induced interactions the  $d \rightarrow c$  and  $s \rightarrow c$  transition have comparable contributions, as the large valence  $d$  quark content of the nucleon compensates for the Cabibbo suppressed  $d \rightarrow c$  transition. Dimuon events in neutrino interactions can be used to measure the strange quark content of the nucleon and the value of the charm quark mass. Moreover, the charm production mechanism is of great importance for testing perturbative QCD predictions.

Neutrino charm production has been investigated with counter experiments like CDHS [1], CCFR [2], CHARM II [3], NOMAD [4] and NuTeV [5], as well as bubble chambers (BEBC [6]) and nuclear emulsion detectors like E531 [7] and CHORUS [8,9,10]. In this paper we present the study of a sample of neutrino induced charged-current dimuon events produced in the lead-scintillating fibre calorimeter of the CHORUS detector; the collected statistics is the second largest to date. The analysis is performed in the framework of the leading order QCD formalism and the result will be expressed in terms of the strange content of the nucleus  $\kappa$ , the charm quark mass  $m_c$ , the Peterson fragmentation parameter  $\epsilon_P$  and the charmed hadron semileptonic branching ratio  $B_\mu$ .

## 1 The CHORUS experiment

The CHORUS experiment has been designed for a short-baseline search of neutrino oscillations in the  $\nu_\mu$ - $\nu_\tau$  channel at relatively high  $\Delta m^2$  [11]. The detector was exposed to the Wide Band Neutrino Beam at CERN from 1995 until 1998. Neutrinos were produced at the SPS by a proton beam of 450 GeV; the average  $\nu_\mu$  energy was 27 GeV with a  $\bar{\nu}_\mu$  contamination of about 6%. The detector is described in detail in Ref. [12]; it consists of a nuclear emulsion target, a fibre tracker, an air gap hadron spectrometer, a lead-scintillating fibre calorimeter and a muon spectrometer.

The 112 ton lead-scintillating fibre calorimeter, described in detail in Ref. [13], consists of three sections (EM, HAD1, HAD2) with decreasing granularity along the beam direction, for a total of 5.2 interaction lengths. Owing to its high mass, the calorimeter also provides an active target for incoming neutrinos. A large number of neutrino charged-current

interactions on lead was collected during the four years of data taking.

A test beam calibration of the calorimeter performances was carried out during the data taking and results are reported in Ref. [13]. Two neural net algorithms were developed in order to improve the vertex position resolution and the energy resolution for charged-current events originating in the calorimeter. Both algorithms have been tuned for the purposes of this analysis on Monte-Carlo neutrino induced events which present more than one reconstructed muon in the final state. The vertex finding algorithm achieved a longitudinal and transverse position resolution of  $\sigma(V_x) = 4.0$  cm and  $\sigma(V_{y,z}) = 3.0$  cm, respectively, with an average efficiency of finding the correct calorimeter plane of  $(82 \pm 1)\%$ . The energy resolution was estimated to be  $\sigma(E_\nu)/E_\nu = 0.39/\sqrt{E_\nu} + 0.14$  (with  $E_\nu$  expressed in GeV).

A muon spectrometer composed of six magnetized iron toroids instrumented with drift chambers and scintillators is located further downstream to identify muons and determine their momentum. A resolution varying from  $\Delta p/p \sim 0.15$  at 20 GeV/ $c$  to  $\Delta p/p \sim 0.19$  at 70 GeV/ $c$  was achieved, as measured with test beam muons.

The trigger system of the CHORUS experiment is described in Ref. [14]. A dedicated muon trigger was set-up to collect a large statistic of “double track” events used both in dimuon and trimuon analyses [15]. A total of  $4.9 \times 10^{19}$  protons were accumulated on the Be target in the period 1995–1998 and the overall CHORUS data collection efficiency was about 92% with a dead time of 5%.

## 2 Theoretical framework

Neutrino interactions with two muons in the final state mainly occur when the weak charged-current on a  $d$  or  $s$  quark produces a charmed quark and the charmed hadron subsequently decays with a probability  $B_\mu$  into a muon and other hadrons. The primary muon and the decay muon have opposite electric charge. The large value of the charm quark mass gives rise to an energy threshold for the process; this is described in the leading order QCD formalism by the so called “slow rescaling” mechanism [16].

### 2.1 Leading order dimuon cross-section

The leading order (LO) QCD framework of deep-inelastic neutrino scattering (DIS) has been adopted to describe charm quark production. This scheme is reported in Ref. [17] and uses the helicity formalism to describe the neutrino charged-current cross-section. It has the advantage of treating in a natural way the different mass scales involved in the heavy

quark production process. The neutrino charm production cross-section is written as

$$\frac{d^2\sigma}{dx dy} = 2G_F^2 \frac{yQ^2}{\pi} (|V_{cd}|^2 d(\chi) + |V_{cs}|^2 s(\chi)) \left[ \left( \frac{1 + \cosh \psi}{2} \right)^2 + \frac{m_c^2}{2Q^2} \frac{\sinh^2 \psi}{2} \right] \quad (1)$$

in terms of the Bjorken variables  $x$  and  $y$  and the Fermi constant  $G_F$ .  $V_{cd}$  and  $V_{cs}$  are the CKM matrix elements,  $d(x)$  and  $s(x)$  being the momentum distributions of the scattered quarks. The angle  $\psi$  is related to  $E_\nu$ ,  $E_\mu$  and  $Q$ , the incoming neutrino energy, the leading muon energy and the  $W$  boson four-momentum, respectively:

$$\cosh \psi = \frac{E_\nu + E_\mu}{\sqrt{Q^2 + (E_\nu - E_\mu)^2}}. \quad (2)$$

This reduces to  $\frac{2-y}{y}$  when  $m_c$  vanishes. With  $m_q$  the mass of the scattered quark and  $M$  the nucleon mass, the scaling variable  $\chi$  is defined as

$$\chi = \eta \frac{(Q^2 - m_q^2 + m_c^2) + \Delta(-Q^2, m_q^2, m_c^2)}{2Q^2}, \quad (3)$$

where

$$\frac{1}{\eta} = \frac{1}{2x} + \sqrt{\frac{1}{4x^2} + \frac{M^2}{Q^2}} \quad (4)$$

and the function  $\Delta$  is given by

$$\Delta(a, b, c) = (a^2 + b^2 + c^2 - 2(ab + bc + ca))^{\frac{1}{2}}. \quad (5)$$

In the limit  $M^2/Q^2 \rightarrow 0$  the variable  $\chi$  becomes the usual ‘‘slow rescaling’’ variable [18].

When dealing with experimentally measured quantities, the expression (1) has to be corrected for the electromagnetic radiative processes arising in the final state whose effect is to lower the primary muon energy and, correspondingly, to raise the hadronic shower energy. A correction for such an effect has been applied according to the prescription of Bardin [19].

## 2.2 Parton distributions

To interpret the experimental data in terms of charm quark production described by Eq. (1) a parametrization of the quark content in the target nuclei is required. The GRV94LO parton distribution functions derived from experimental deep-inelastic scattering data has been used [20]. To take into account the non-isoscalarity of the lead-scintillating fibre calorimeter, the total valence quark content has been parametrized as

$$x q_{\text{val}}(x, Q^2) = \frac{A-Z}{A} x u_{\text{val}} + \frac{Z}{A} x d_{\text{val}} , \quad (6)$$

where, due to strong isospin symmetry, the *down* quark content of the neutron is taken to be the same as the *up* quark content of the proton. The strange quark content in protons and neutrons is assumed to be the same. The non-strange sea-quark contents of the nucleon is assumed to be symmetric between up and down quarks. The strange quark content of the nucleon is described by the parameter

$$\kappa = \frac{\int [xs(x, \mu_o^2) + x\bar{s}(x, \mu_o^2)] dx}{\int [x\bar{u}(x, \mu_o^2) + x\bar{d}(x, \mu_o^2)] dx} , \quad (7)$$

where  $\mu_o^2$  is an arbitrary reference scale chosen to be 20 GeV<sup>2</sup>. In the following, an SU(3) flavour symmetric sea is assumed; this means that the strange and the anti-strange content of the nucleon are the same and have the same  $x$  dependence.

An additional parameter  $\alpha$  is often introduced in similar analyses that allows the strange quark to behave differently from the up and down quarks. This is obtained by multiplying the strange quark parton distribution function (*pdf*) by the factor  $(1-x)^\alpha$ . In the following the weighted average  $\alpha = 2 \pm 1$  of the values given by the CHARM II and CCFR leading order analyses is used.

## 2.3 Charm quark fragmentation and meson decays

The non-perturbative processes that act to “dress” the bare charm quark produced in the neutrino interaction are known as fragmentation or hadronization. The fragmentation is usually described as a function of the variable  $z$  defined as the fraction of the longitudinal momentum taken over by the charm hadron  $h_c$ :

$$z = P_L(h_c)/P_L^{\text{max}}(h_c) , \quad (8)$$

where  $P_L^{\max}(h_c)$  is the maximum hadron longitudinal momentum relative to the W-boson direction in the boson-nucleon center of mass reference frame. The Peterson parametrization of the charm quark fragmentation is written as [21]

$$D(z, \epsilon_P) \propto z^{-1} \left( 1 - \frac{1}{z} - \frac{\epsilon_P}{1-z} \right)^{-2}, \quad (9)$$

where  $\epsilon_P$  is a free parameter to be determined from the data. In leading order QCD, the neutrino cross-section can be factorized as

$$\frac{d^3\sigma_\nu}{dx dy dz}(\nu N \rightarrow \mu h_c X) = \frac{d^3\sigma_\nu^{LO}}{dx dy dz}(\nu N \rightarrow \mu c X) D(z). \quad (10)$$

This is no longer true in the next-to-leading order formalism [22]. The transverse momentum of charmed hadrons with respect to the W-boson direction is on average small ( $\langle p_T^2 \rangle \sim 0.2 \text{ GeV}^2/c^2$ ) and is assumed to be distributed as  $dN/dp_T^2 \propto e^{-bp_T^2}$ . The parameter  $b$  is taken to be  $1.1 \text{ GeV}^2/c^2$  following Ref. [23].

The fragmentation variable  $z$  cannot be determined on an event-by-event basis since the direction of the charm quark or charmed hadron cannot be measured directly. The visible fragmentation variable is thus defined as

$$z_{\text{vis}} = \frac{E_{\mu 2}}{(E_{\mu 2} + E_{\text{sh}})}, \quad (11)$$

where  $E_{\mu 2}$  and  $E_{\text{sh}}$  are the energy of the muon coming from the charmed hadron decay and the hadronic shower final state energy, respectively. The relation between  $z$  and  $z_{\text{vis}}$  has been studied with the aid of Monte-Carlo simulations.

### 3 Data sample and event selection

The dimuon sample was collected during four years of data taking using a dedicated trigger setup based on the energy released in the fibre calorimeter and on the presence of two or more well separated tracks in the spectrometer [14]. A total of  $6.6 \times 10^6$  events tagged as dimuons by the trigger were reduced to about  $5.0 \times 10^5$  requiring that at least two muons were well reconstructed in the muon spectrometer. For each event, the reconstructed muon energy  $E_\mu$ , the angle of the muon with respect to the neutrino beam direction  $\theta_\mu$  evaluated at the interaction vertex and the hadron shower energy  $E_{\text{sh}}$  are used to derive the following kinematic variables:

- $E_\nu^{\text{vis}} = E_{\text{sh}} + E_{\mu 1} + E_{\mu 2}$ , the visible neutrino energy

- $Q_{\text{vis}}^2 = 2E_{\nu}^{\text{vis}}E_{\mu 1}(1 - \cos \theta_{\mu 1}) - m_{\mu}^2$ , the visible four-momentum transfer squared
- $x_{\text{vis}} = Q_{\text{vis}}^2/2M(E_{\text{sh}} + E_{\mu 2})$ , the visible Bjorken  $x$
- $z_{\text{vis}} = E_{\mu 2}/(E_{\text{sh}} + E_{\mu 2})$ , the visible fragmentation variable, as reported in Eq. 11.

The final sample of dimuon events was selected imposing the following selection criteria:

- C1: at least two muons must be well reconstructed, i.e. a minimum of five measured track points in the drift chambers placed in the gaps between the iron magnets is required for both muons;
- C2: the longitudinal position of the event vertex ( $V_x$ ) determined by the Neural Net algorithm must be inside a fiducial volume given by  $290.7 \text{ cm} < V_x < 384.0 \text{ cm}$  (this corresponds mainly to the HAD1 part of the calorimeter); the transverse vertex positions ( $V_y$  and  $V_z$ ) are required to satisfy  $-120 \text{ cm} < V_{y,z} < 120 \text{ cm}$  to ensure hadronic shower lateral containment;
- C3: the shower energy must be in the range  $5 \text{ GeV} < E_{\text{sh}} < 150 \text{ GeV}$ ;
- C4: to ensure a good reconstruction quality and control of the acceptances, a cut  $E_{\mu} > 5 \text{ GeV}$  when extrapolated to the vertex position in the calorimeter is applied. This cut also reduces the meson decay background;
- C5: the reconstructed neutrino energy must be in the range  $10 \text{ GeV} < E_{\nu} < 240 \text{ GeV}$  to ensure a good control of the detection efficiencies;
- C6: a cut  $Q^2 > 3.0 \text{ GeV}^2/c^2$  is applied in order to exclude regions in which the Monte-Carlo simulation is not reliable, as described in the following section;
- C7: the transverse distance between the two muons extrapolated to the interaction vertex  $x$  coordinate ( $d_{12}$ ) is requested to be less than 15 cm to reject background due to hadron decays.

The primary muon is assumed to be the one with the highest  $p_T$  with respect to the neutrino beam direction; this leads to a  $(95.8 \pm 1.0)\%$  efficiency to correctly identify the primary muon for neutrino induced interactions and  $(94.0 \pm 1.1)\%$  for antineutrino interactions. In cases in which there are more than two reconstructed muons, the two most energetic ones are used in the analysis. The average charm induced opposite sign dimuon trigger efficiency was evaluated by means of Monte-Carlo simulation on a sample of events surviving the selection cuts and found to be  $(91 \pm 6)\%$ . The event statistics is reported in Table 1 where the top line indicates the charges of the primary and secondary muons respectively.

The dimuon sample statistics after the selection is therefore

$$N^{-+} = 10218 ; N^{--} = 1441 ; N^{+-} = 975 ; N^{++} = 46 . \quad (12)$$

Figure 1 shows a scatter plot of the selected events in the  $(p_{\mu 1}, p_{\mu 2})$  plane.

Table 1

Statistics for opposite-sign and same-sign dimuon events induced by neutrino interactions. The cuts are explained in the text.

Cut	--+	--	+--	++	total
C1	33251	30750	5769	899	70669
C2	17517	12387	2144	203	32251
C3	16894	11510	2023	186	30613
C4	13948	10078	1689	141	25856
C5	13938	10051	1688	140	25817
C6	12579	8962	1270	110	22921
C7	10218	1441	975	46	12680

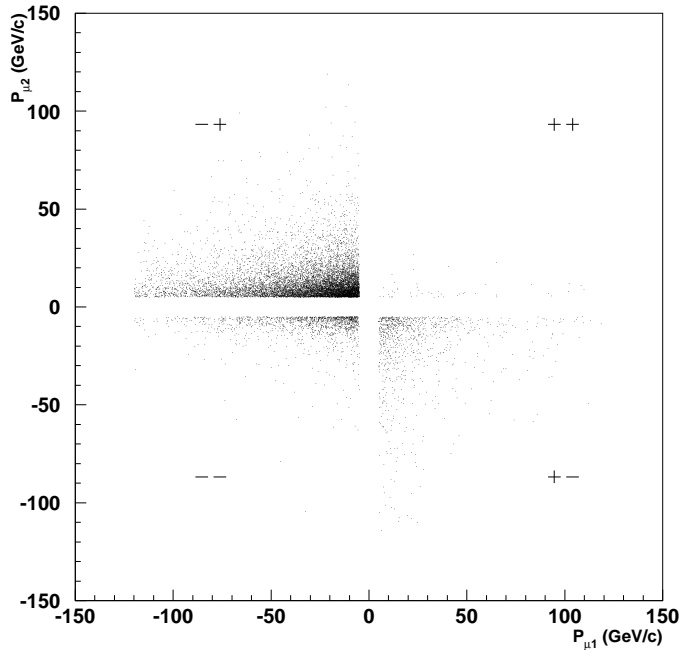


Fig. 1. Scatter plot in the  $(p_{\mu_1}, p_{\mu_2})$  plane of the dimuon selected events. The sign of the muon momentum represents its electric charge.

#### 4 Monte-Carlo simulation

A full simulation of the events induced by neutrinos with the production of a charmed quark has been performed. The first step of the simulation consists in the implementation of the formalism described in section 2. A specific event generator has been developed by

the CHORUS collaboration. It implements JETSET [24] for charm quark fragmentation and charmed hadron decays following Eq. (9). The incoming neutrino beam is described according to a GEANT 3.21 [25] based package that describes the interaction of the SPS proton beam with the beryllium target. All relevant components of the beam were part of the simulation. The parton distribution functions were implemented with the use of the PDFLIB [26] package. The GRV94LO [20] *pdf*'s were adopted in the production of the sample of events used in the fit procedure. The CTEQ3L [27] *pdf*'s have been used to obtain an estimate of the systematic error on the final result. The value of the CKM mixing matrix elements has been taken from the PDG compilation [28]. The maximum allowed incoming neutrino energy was  $E_\nu^{\max} = 300$  GeV and the kinematical bounds in the event generator were  $Q_{\min}^2 = 2.0$  GeV<sup>2</sup>/c<sup>2</sup> and  $W_{\min}^2 = 4.0$  GeV<sup>2</sup> in order to avoid quasi-elastic and resonance production processes.

The generator output is then used as input for the CHORUS event simulation program. Based on GEANT 3.21 [25], it contains the complete description of the apparatus and provides the response of the various instrumented parts of the detector. The events produced in this way undergo all the analysis steps performed for the real data.

#### 4.1 Background evaluation

The main source of background to the charm induced dimuon events is given by the muonic decay of non-charmed hadrons produced either directly or during the shower development of a charged-current event. The background level depends on the probability for a  $\pi^\pm$  or a  $K^\pm$  to decay before it interacts in the calorimeter or in the first part of the muon spectrometer. The relative rates of same-sign and opposite-sign events resulting from this background are closely related to the probability of producing positive or negative pions and kaons during the hadronic shower development. A standard way to estimate its contribution to the opposite-sign dimuon sample relies on the admitted hypothesis that the same-sign dimuon events belong to the background. For instance, the background to the charm induced opposite-sign dimuon events with a leading  $\mu^-$  is given by

$$B^{-+} = \left( \frac{N_{CC}^{-+}}{N_{CC}^{--}} \right)_{MC} \times N_{DATA}^{--} . \quad (13)$$

where the charm to muon decay process has been disabled in the simulation of the neutrino induced charged-current events. A total of about 300 events were obtained after selection cuts out of  $3 \times 10^6$  neutrino CC interactions for which a complete MonteCarlo simulation of the detector response has been performed. The comparison between same-sign neutrino dimuon events in data and MonteCarlo is shown in Figure 2; the fairly good agreement between data and MonteCarlo validates the use of relation (13). Using this sample of events, a value of  $(N_{CC}^{-+}/N_{CC}^{--})_{MC} = 0.89 \pm 0.10$  has been established. Once selection cuts have

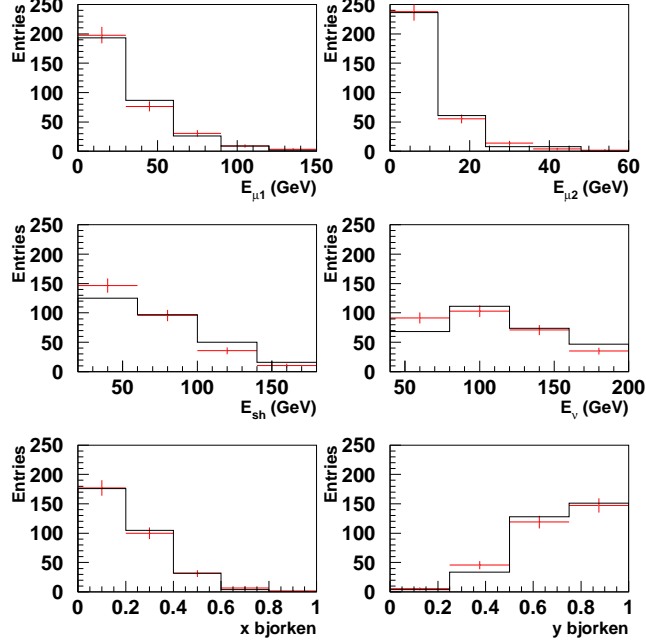


Fig. 2. Comparison between reconstructed quantities for same-sign dimuon events in data (points) and MC sample (histogram).

been applied, the number of events with opposite sign dimuons is thus smaller than that of same sign muons<sup>1</sup>; this is mainly due to the fact that the magnet polarity of the muon spectrometer was chosen to focus negative charged muons. Consequently, the efficiency to reconstruct a  $\mu^+$  is smaller than to reconstruct a  $\mu^-$ . The majority of background events is in the region of small muon energy where the effect is more pronounced. Similarly the value  $(N_{CC}^{+-}/N_{CC}^{--})_{MC} = 0.11 \pm 0.02$  is obtained and used to evaluate the non-charm background to the opposite-sign dimuon sample with a leading  $\mu^+$ .

## 5 Results

The number of observed dimuon events depends on the charm quark mass ( $m_c$ ) via the slow rescaling mechanism, the amount of strange quark sea ( $\kappa$ ), the fragmentation parameter ( $\epsilon_P$ ) and on the branching ratio of charm into muon ( $B_\mu$ ). From the initial sample of Table 1, taking into account selection efficiencies and neutrino–antineutrino cross contamination, a

<sup>1</sup> The ratios between positive and negative pions and kaons produced in the MonteCarlo sample of neutrino induced charged current interactions are  $\pi^+/\pi^- \sim 1.7$  and  $K^+/K^- \sim 1.6$  for events having  $E_{\mu 1} > 10$  GeV and  $E_{\pi, K} > 5$  GeV

Table 2

Results of the four parameter fit procedure and parameter correlation matrix given by MINUIT.

	Fit result		Parameter Correlation Coefficients				
	value	error	Global	$m_c[\text{GeV}/c^2]$	$\kappa$	$\epsilon_P$	$B_\mu$
$m_c[\text{GeV}/c^2]$	1.258	0.160	0.74986	1.000	0.522	-0.732	0.018
$\kappa$	0.326	0.048	0.56786	0.522	1.000	-0.534	-0.018
$\epsilon_P$	0.0646	0.0053	0.75471	-0.732	-0.534	1.000	0.031
$B_\mu$	0.0959	0.0038	0.06935	0.018	-0.018	0.031	1.000

total of  $8910 \pm 180$  events with a leading  $\mu^-$  and  $430 \pm 60$  events with a leading  $\mu^+$  were selected. This represents the second largest sample of neutrino induced dimuons to date.

### 5.1 Maximum Likelihood four-parameter fit

To extract information on the production mechanism of dimuon events, a maximum likelihood fit of the Monte-Carlo events to the data has been performed.

A Monte-Carlo reference sample has been used to avoid the painful procedure in which the likelihood is evaluated by generating a different sample of events for each set of parameters. The charm quark mass was set to  $m_c^{\text{ref}} = 0.5 \text{ GeV}/c^2$  to avoid a possible bias due to the vanishing charm production cross-section below the  $m_c^{\text{ref}}$  value, while the other parameters were set to  $\kappa^{\text{ref}} = 0.45$  and  $\epsilon_P^{\text{ref}} = 0.07$ . All Monte-Carlo “true” information has been retained to be able to weight each event when any of the four parameters is changed during the fitting procedure. The reference sample consists of 17439 events that survived the selection criteria out of  $3.5 \times 10^5$  fully reconstructed generated events.

An unbinned likelihood fit of the four unknown parameters has been performed on the basis of the distributions of the three experimental observables  $E_\nu^{\text{vis}}$ ,  $x_{\text{vis}}$  and  $z_{\text{vis}}$ . The probability density functions of the three observables are constructed by assigning to each event in the reference sample a weight equal to the ratio of the cross-section evaluated with the current set of parameters to the cross-section obtained with the reference set. The absolute normalization of the Monte-Carlo sample was obtained by using the observed dimuon production rate with respect to the single muon events and fixing the absolute value of the cross-section with the same method as reported in Ref. [29].

The fit was performed using MINUIT [30] simultaneously on the four unknown parameters and the result of the fit procedure is reported in Table 2. Figures 3 and 4 show the comparison between the data and the Monte-Carlo samples produced using the best fit values reported in Table 2. The result of the fit is very stable and consistent values are obtained by fitting separately each parameter keeping the others fixed.

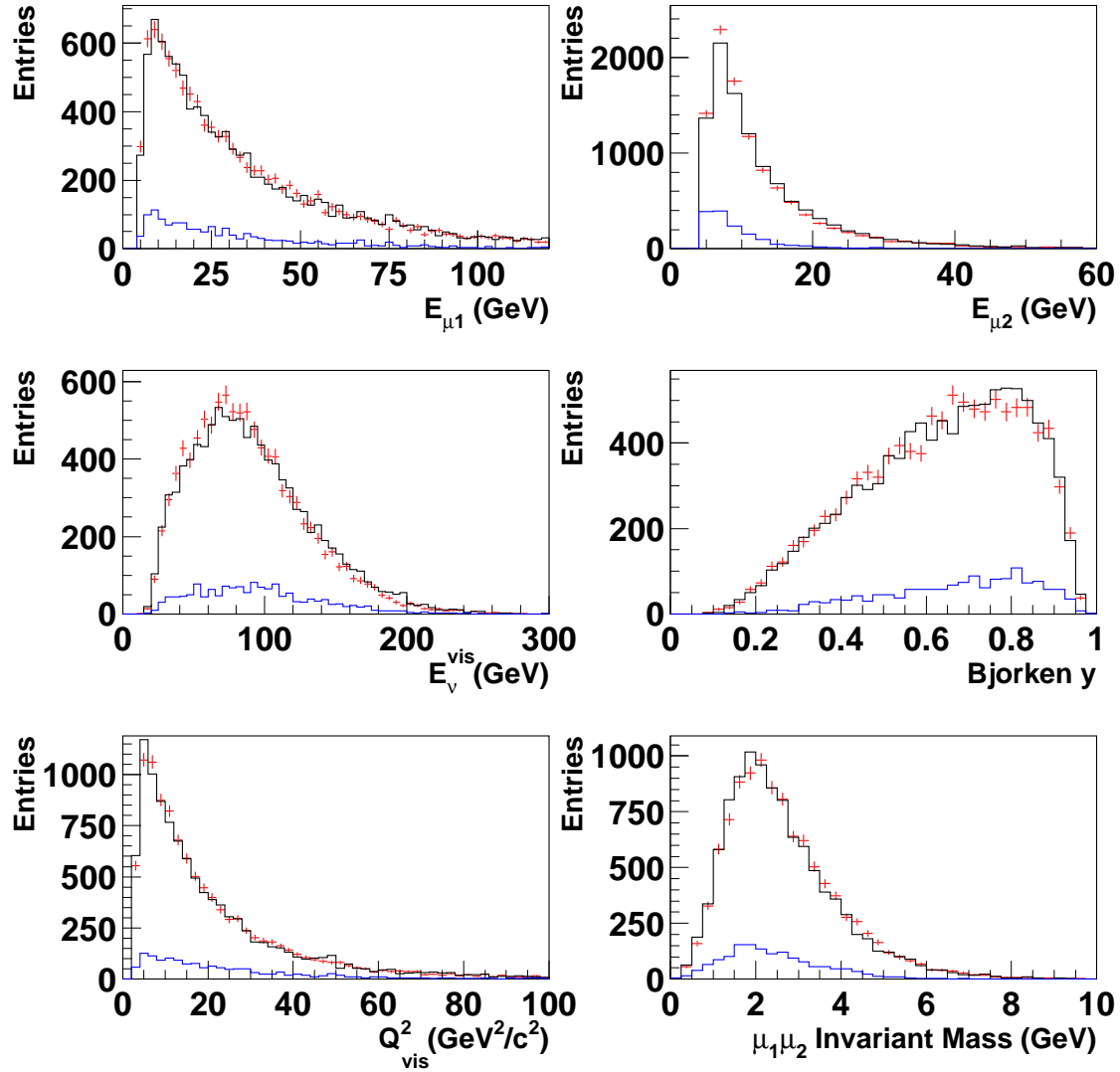


Fig. 3. Comparison between data (points) and Monte-Carlo (histogram) evaluated using the parameters found by the fit procedure. The small fraction of events originating from pions and kaons decaying into muons is also shown.

## 5.2 Systematic uncertainties

Systematic uncertainties on the result of the fit are mainly due to the theoretical model, the background description and the neutrino flux normalization. Theoretical uncertainties were taken as the maximum deviation of each fitted value from its central value when varying the parameters of the model inside their quoted errors and repeating the fit proce-

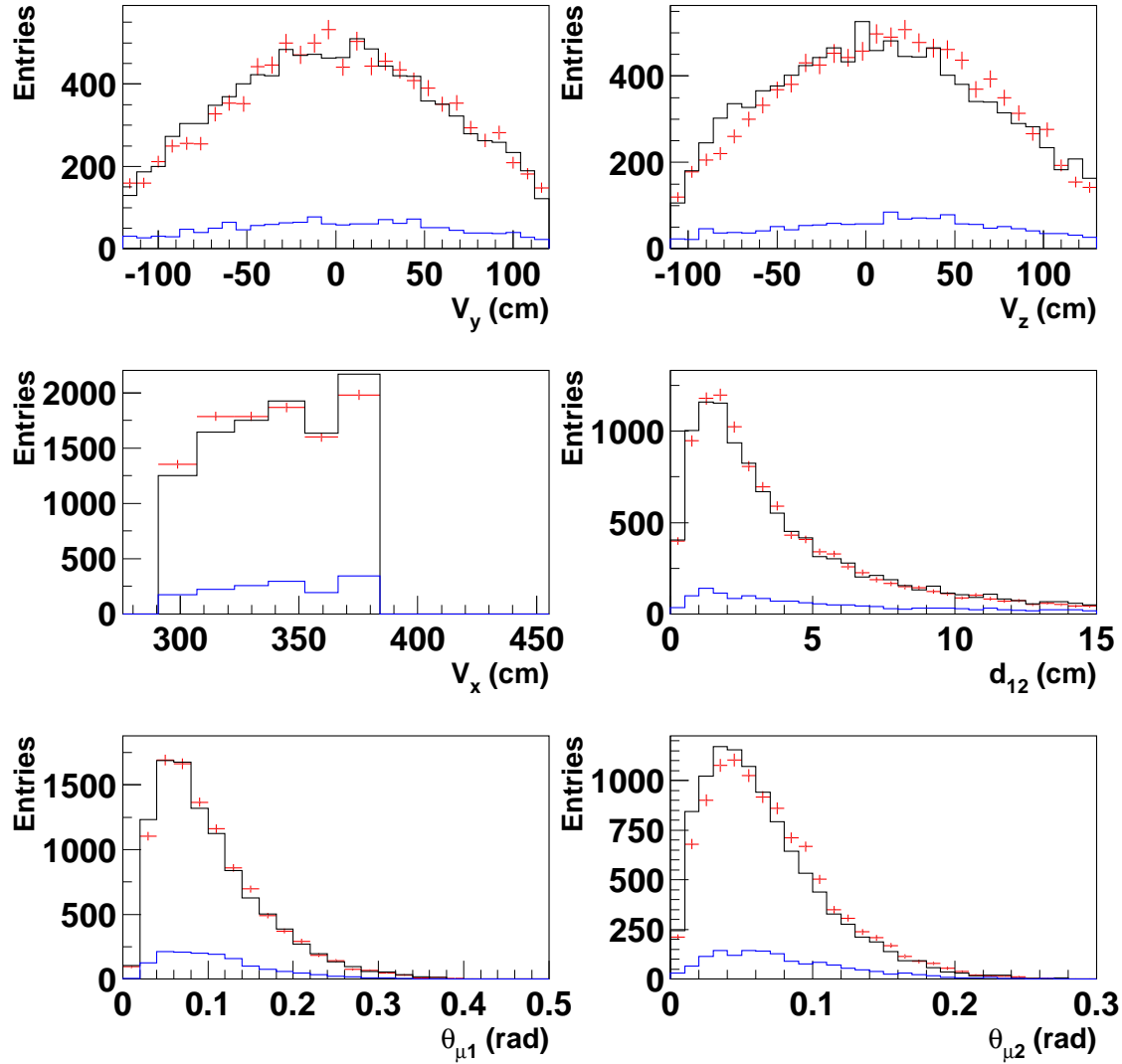


Fig. 4. Comparison between data (points) and Monte-Carlo (histogram) evaluated using the parameters found by the fit procedure. The small fraction of events originating from pions and kaons decaying into muon is also shown.

cedure. The contribution of the nucleon  $pdf$  has been evaluated repeating the fit procedure using the CTEQ3L  $pdf$  parametrization. The amount of events induced by pion and kaon decays, the background subtraction procedure and the total uncertainty on the overall event normalization set the limit on the precision of  $B_\mu$  and of the ratio of the dimuon to the charged-current cross-sections  $\sigma_{-+}/\sigma_{CC}$ . The systematic errors due to the fiducial volume and the event selection criteria definition have been evaluated by varying these cuts inside the resolutions of the corresponding variables. The major contributions to the

Table 3

Major sources of systematic error uncertainties to the evaluated values of  $m_c$ ,  $\kappa$  and  $\epsilon_P$  and  $B_\mu$ .

	$\Delta m_c$ [GeV/ $c^2$ ]	$\Delta \kappa$	$\Delta \epsilon_P$	$\Delta B_\mu$
$m_c$ [GeV/ $c^2$ ]	—	0.02	0.004	0.001
$\kappa$	0.02	—	0.005	0.001
$\epsilon_P$	0.03	0.02	—	0.001
Event normalization	—	—	—	0.003
Background scale	0.04	0.02	0.004	0.005
Fit procedure	0.01	0.002	0.001	0.0005
$E_{\text{sh}}$ scale (5%)	0.03	0.013	0.001	0.004
$E_{\text{sh}}$ offset ( $\pm 2$ GeV)	0.05	0.011	0.001	0.001
Radiative corrections	0.02	0.005	0.002	0.0005
$V_{\text{cd}}$ , $V_{\text{cs}}$ , nucleon <i>pdf</i>	0.02	0.015	0.001	0.002
Fiducial volume	0.01	0.02	0.001	0.0012
Selection cuts	0.02	0.003	0.002	0.0011
Total	0.088	0.046	0.0084	0.0078

total systematic errors on the four fitted parameters are shown in Table 3.

Including the systematic uncertainties, the result of this leading order analysis can be summarized as follows:

$$\begin{aligned}
 m_c &= (1.26 \pm 0.16(\text{stat}) \pm 0.09(\text{syst})) \text{ GeV}/c^2 \\
 \kappa &= 0.33 \pm 0.05(\text{stat}) \pm 0.05(\text{syst}) \\
 \epsilon_P &= 0.065 \pm 0.005(\text{stat}) \pm 0.009(\text{syst}) \\
 B_\mu &= 0.096 \pm 0.004(\text{stat}) \pm 0.008(\text{syst})
 \end{aligned}
 \tag{14}$$

## 6 Discussion and conclusions

The results of this analysis are in agreement with those reported by previous experiments [1,2,3,4,5], as shown in Table 4.

The value of  $B_\mu |V_{\text{cd}}|^2$  obtained using the results of this analysis can be combined directly with other leading order results [1,2,3] following the prescription given in Ref. [31]. An

average value of

$$(B_\mu|V_{cd}|^2)_{\text{LO}} = (0.474 \pm 0.027) \times 10^{-2} \quad (15)$$

is obtained.

Results of this analysis may also be compared with earlier analyses of events originating in the nuclear emulsion target of the CHORUS experiment. Good agreement is found with the result  $B_\mu = 0.085 \pm 0.010$  obtained after applying the selection  $E_\nu > 30 \text{ GeV}/c$  [10]. The use of that selection for the comparison is justified by the small contribution of events below 30 GeV in the present analysis, as visible in Fig. 3. The value of the Peterson fragmentation parameter  $\epsilon_P = 0.059 \pm 0.013$  reported in Ref. [8] for the same definition of  $z$  as used here (called  $\epsilon_P^Q$  in Ref. [8]) is in good agreement with the result found in the present analysis. In Ref. [9], the value  $m_c = (1.42 \pm 0.08) \text{ GeV}/c^2$  was reported, assuming  $\kappa = 0.38$  and  $\alpha = 1$ . The dependence of  $m_c$  on  $\kappa$  and  $\alpha$  is given in Ref. [8]. For  $\alpha = 2$ , as used here, and fixing  $\kappa$  to its fitted value 0.33, the value of  $m_c$  becomes  $1.30 \pm 0.08 \text{ GeV}/c^2$  in excellent agreement with the value found in the present analysis.

As an additional result, the large sample of collected dimuon events allowed us to make the evaluation of the rate of charm induced opposite-sign dimuon events relative to the charged-current events as a function of the incoming neutrino energy. An unfolding procedure has been used to take into account all detector effects. The correlation between different energy bins has been evaluated using a Monte-Carlo simulation. The correction due to the missing energy of the outgoing neutrino in the charm decay has been calculated for each energy bin using the Monte-Carlo event sample. The result is shown in Fig. 5 where statistical and systematic errors have been added in quadrature. It agrees well with the world average dimuon rate shown in Fig.26 of Ref. [31].

In summary, the analysis of the second largest sample of neutrino induced dimuon events has been performed using a leading order QCD formalism. The slow rescaling mechanism gives a good description of the CHORUS data. Results on the charm quark mass  $m_c$ , the

Table 4

Compilation of latest results on neutrino induced opposite-sign dimuon events.

Experiment	$N_{2\mu}(\nu)$	$N_{2\mu}(\bar{\nu})$	$m_c$ [GeV/ $c^2$ ]	$\kappa$	$B_\mu$	$\epsilon_P$
This analysis	8910	430	$1.26 \pm 0.18$	$0.33 \pm 0.07$	$0.096 \pm 0.008$	$0.065 \pm 0.010$
CDHS [1]	9922	2123	—	$0.47 \pm 0.09$	$0.084 \pm 0.014$	[0.02, 0.14]
CCFR [2]	4503	632	$1.3 \pm 0.2$	$0.44 \pm 0.09$	$0.109 \pm 0.010$	—
CHARM II [3]	3100	700	$1.8 \pm 0.4$	$0.39 \pm 0.09$	$0.091 \pm 0.010$	$0.072 \pm 0.017$
NOMAD [4]	2714	115	$1.3 \pm 0.4$	$0.48 \pm 0.17$	$0.095 \pm 0.015$	$0.08 \pm 0.05$
NuTeV [5]	2280	655	$1.3 \pm 0.2$	$0.38 \pm 0.08$	$0.101 \pm 0.012$	—

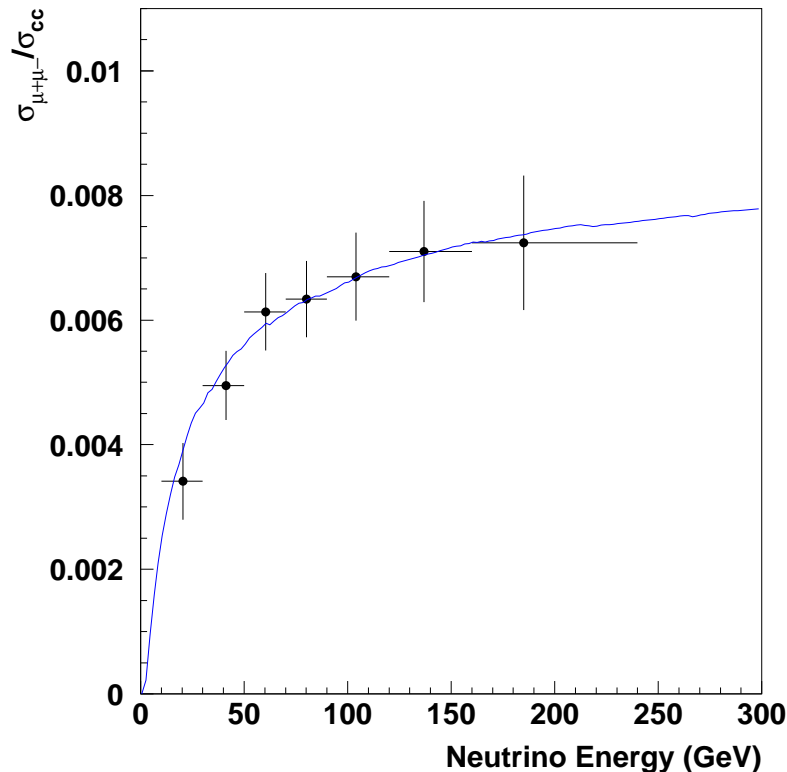


Fig. 5. Opposite-sign dimuon production relative cross-section. The solid line represents the Monte-Carlo prediction obtained using the values of Table 2.

content of strange quark in the nucleon  $\kappa$ , the Peterson fragmentation parameter  $\epsilon_P$  and the branching fraction of charmed hadrons into muon,  $B_\mu$ , agree with the data obtained in similar analyses and improve the overall knowledge on the neutrino induced charm production and charm decay mechanisms.

## 7 Acknowledgments

We gratefully acknowledge the help and support of the neutrino beam staff and of the numerous technical collaborators who contributed to the detector construction and operation. The experiment was made possible by grants from the Institut Interuniversitaire des Sciences Nucléaires and the Interuniversitair Instituut voor Kernwetenschappen (Belgium), the Israel Science Foundation (grant 328/94) and the Technion Vice President Fund for the Promotion of Research (Israel), CERN (Geneve, Switzerland), the German Bundesministerium für Bildung und Forschung (Germany), the Institute of Theoretical and Experimental Physics (Moscow, Russia), the Istituto Nazionale di Fisica Nucleare (Italy),

the Promotion and Mutual Aid Corporation for Private Schools of Japan and Japan Society for the Promotion of Science (Japan), the Korea Research Foundation Grant (KRF-2003-005-C00014) (Republic of Korea), the Foundation for Fundamental Research Organization NWO (The Netherlands), and the Scientific and Technical Research Council of Turkey (Turkey). We gratefully acknowledge their support.

## References

- [1] H. Abramowicz *et al.*, Z. Phys. **C15** (1982) 19.
- [2] S.A. Rabinowitz *et al.*, Phys. Rev. Lett. **70** (1993) 134;  
A.O. Bazarko *et al.*, Z. Phys. **C65** (1995) 189.
- [3] P. Vilain *et al.*, Eur. Phys. J. **C11** (1999) 19-34.
- [4] P. Astier *et al.*, Phys. Lett. **B486** (2000) 35-48.
- [5] M. Goncharov *et al.*, Phys. Rev. **D64** (2001) 112006.
- [6] G. Gerbier *et al.*, Z. Phys. **C29** (1985) 15.
- [7] N. Ushida *et al.*, Phys. Lett. **B121** (1983) 292.
- [8] G. Önençut *et al.*, Phys. Lett. **B604** (2004) 145-156.
- [9] G. Önençut *et al.*, Phys. Lett. **B613** (2005) 105-117.
- [10] A. Kayis-Topaksu *et al.*, Phys. Lett. **B626** (2005) 24-34.
- [11] E. Eskut *et al.*, Phys. Lett. **B497** (2001) 8-22.
- [12] E. Eskut *et al.*, Nucl. Inst. and Methods **A401** (1997) 7.
- [13] E. Di Capua *et al.*, Nucl. Inst. and Methods **A378** (1996) 221.
- [14] M.G. van Beuzekom *et al.*, Nucl. Inst. and Methods **A427** (1999) 587.
- [15] A. Kayis-Topaksu *et al.*, Phys. Lett. **B596** (2004) 44-53.
- [16] H. Georgi and H.D. Politzer *et al.*, Phys. Rev. **D14** (1976) 1829.
- [17] M.A.G. Aivazis *et al.*, Phys. Rev. **D50** (1994) 3085; M.A.G. Aivazis *et al.*, Phys. Rev. **D50** (1994) 3102.
- [18] R.M. Barnett, Phys. Rev. Lett. **36** (1976) 1163.
- [19] D.Yu. Bardin and V.A. Dokuchaeva, Preprint JINR E2-86-260 (1986).
- [20] M. Glück, E. Reya and A. Vogt, Z. Phys. **C67** (1995) 433-448.

- [21] C. Peterson *et al.*, Phys. Rev. **D27** (1983) 105.
- [22] M. Glück *et al.*, Phys. Lett. **B398** (1997) 391.
- [23] M. Aguilar-Benitez *et al.*, Phys. Lett. **B123** (1983) 98.
- [24] T. Sjostrand, Comput. Phys. Commun. **82** (1994) 74.
- [25] GEANT 3.21, CERN program library long writeup W5013.
- [26] H. Plochow-Besch, PDFLIB, CERN program library long writeup W5051.
- [27] H.L. Lai *et al.*, Phys. Rev. **D51** (1995) 4763.
- [28] S. Eidelman *et al.*, Phys. Lett. **B592** (2004) 1.
- [29] G. Önençüt *et al.*, Phys. Lett. **B632** (2006) 65-75.
- [30] F. James, MINUIT:Function Minimization and Error Analysis, CERN program library entry D506.
- [31] P. Migliozi *et al.*, Phys. Rep. **399** (2004) 227-320.